

Electrochemical and Computational Studies of Proline and Captopril as Corrosion Inhibitors on Carbon Steel in a Phase Change Material Solution

Wenwu Li¹, Zhe Zhang^{1,2,*}, Ying Zhai¹, Le Ruan^{1,2,**}, Weipeng Zhang¹, Ling Wu³

¹ Guangxi Key Laboratory of Electrochemical and Magneto-chemical Functional Materials, College of Chemistry and Bioengineering, Guilin University of Technology, Guilin 541004, PR China

² Guangxi Key Laboratory of Geomechanics and Geotechnical Engineering, Guilin University of Technology, Guilin 541004, PR China

³ School of Chemistry and Chemical Engineering, Shandong University, Jinan 250100, PR China

*E-mail: zhangzhe@glut.edu.cn

**E-mail: ruanle@glut.edu.cn

Received: 17 August 2019 / Accepted: 19 October 2019 / Published: 30 November 2019

In this paper, electrochemical and surface analysis methods were used to study the corrosion inhibition performance of proline and captopril on 1045 carbon steel in phase change materials (PCMs). From the electrochemical impedance spectroscopy test results, both proline and captopril inhibitors have a corrosion inhibition effect on 1045 carbon steel in PCM solution, but captopril inhibitors (concentration=0.0005 mol·L⁻¹) have a better inhibition efficiency ($\eta_{\max}=92.73\%$) than that of proline. The results of the potentiodynamic polarization tests show that both proline and captopril are mixed type corrosion inhibitors. Field emission scanning electron microscopy (FESEM) and contact angle test results show that captopril inhibitors can effectively reduce the corrosion degree of carbon steel in PCMs. The inhibition mechanism of proline and captopril inhibitors was analysed by theoretical calculations. Both corrosion inhibitor molecules can adsorb on the Fe(1 1 0) surface, among which N atoms, S atoms and -COOH groups are the main sites of adsorption activity. In addition, the diffusion coefficients and surface concentration profiles of H₂O molecules and Cl⁻ ions in the two corrosion inhibition systems were studied by a molecular dynamics simulation, which verified that captopril corrosion inhibitors have good corrosion inhibition effects.

Keywords: Carbon steel; Inhibition; Electrochemical measurements; Computational

1. INTRODUCTION

In recent years, energy shortages and environmental pollution have become important issues. An effective use of renewable energy and an improvement in energy efficiency in industrial

development is extremely urgent. Therefore, phase change materials (PCMs) have become a research hotspot in the field of international energy utilization and materials science[1-8]. PCMs are mixed solutions of highly concentrated ions composed of inorganic salts, water, etc., which can absorb heat from the environment or release heat to the environment; that is accomplished by utilizing the phase or structural changes of the materials themselves within a certain temperature range[9]. PCMs have the characteristics of high energy storage density and high thermal conductivity, along with an easily controlled process. Thermal energy storage technology using PCMs is a notable way to improve the efficiency of thermal energy conversion and recycling, and is also an effective way to store renewable energy. However, there are higher concentrations of corrosive ions in widely used hydrated salt phase change materials, which eventually cause severe corrosion and damage to metal container[10-14]. To make PCMs better developed for application, it is important in this field to study the corrosion mechanism of PCMs on metal containers and to explore ways to reduce that metal corrosion. At present, there are few ways to slow down the corrosion of metal in PCM, and most researchers are searching for metal materials with high corrosion resistance. Eduard Oró et al.[15] studied the corrosive effects of different metals and polymers in contact with certain PCMs used in cryogenic applications. The results show that 316 stainless steel, PP, PS, PET and HDPE are more suitable for use as PCM container materials than PCM containers made from copper and carbon steel. Maria C. Browne et al.[16] used immersion etching to study the compatibility of PCM with various materials for thermal energy storage (TES) applications. The results show that stainless steel can be used in all PCMs under investigation. Pere et al.[17] studied the corrosive effects of two metals and two alloys in contact with eleven PCMs used in high and low temperature applications. The results show that stainless steel is suitable for $\text{NaOH}\cdot 1.5\text{H}_2\text{O}$, $\text{ZnCl}_2\cdot 3\text{H}_2\text{O}$, $\text{K}_2\text{HPO}_4\cdot 6\text{H}_2\text{O}$, commercial PCM S10 and C10. Carbon steel is suitable for $\text{NaOH}\cdot 1.5\text{H}_2\text{O}$, $\text{K}_3\text{PO}_4\cdot 7\text{H}_2\text{O}$ and commercial PCM C48. Copper is suitable for $\text{ZnCl}_2\cdot 3\text{H}_2\text{O}$ and $\text{K}_2\text{HPO}_4\cdot 6\text{H}_2\text{O}$. Additionally, aluminum has good compatibility with $\text{MgSO}_4\cdot 7\text{H}_2\text{O}$, commercial PCM C48 and C10.

With the increasing market demand for environmentally friendly corrosion inhibitors, amino acids with good solubility, low price, and wide availability, along with being non-toxic and harmless to the environment and human beings have been widely used in the field of corrosion protection[18-23]. In this paper, proline and captopril were selected as corrosion inhibitors. Electrochemical testing, FESEM characterization, contact angle testing, quantum chemical calculations and molecular dynamics simulations were used to study the corrosion inhibition performance and mechanism of the corrosion inhibitors on carbon steel in PCMs.

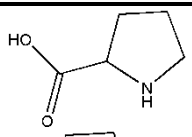
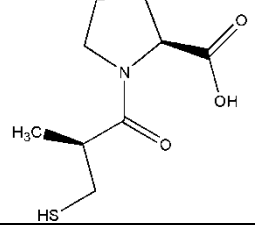
2. EXPERIMENTS

2.1. Inhibitors and solutions

The corrosion inhibitors used in the experiments were proline and captopril from Shanghai Macklin Biochemical Co. Ltd. Details of the molecular structure of the two corrosion inhibitors are shown in Table 1. The composition of the PCM solution is sodium sulfate decahydrate (43.2 wt.%,

main phase change material), disodium hydrogen phosphate dodecahydrate (12.3 wt.%, main phase change material), ammonium chloride (6.2 wt.%, pour point depressant), potassium chloride (3.1 wt.%, pour point depressant), ammonium dihydrogen phosphate (3.1 wt.%, pH buffer), borax (1.9 wt.%, nucleating agent), CMC (2.5 wt.%, flocculant) and distilled water (27.8 wt.%, solvent). The test concentrations of the two corrosion inhibitors were $0 \text{ mol}\cdot\text{L}^{-1}$, $0.0001 \text{ mol}\cdot\text{L}^{-1}$, $0.0005 \text{ mol}\cdot\text{L}^{-1}$, $0.001 \text{ mol}\cdot\text{L}^{-1}$, $0.005 \text{ mol}\cdot\text{L}^{-1}$ and $0.01 \text{ mol}\cdot\text{L}^{-1}$. In addition, a cooling curve analysis was performed on PCMs with and without corrosion inhibitor. As shown in Fig. 1, the test results show that the two corrosion inhibitors have no significant effect on the PCM thermal properties.

Table 1. Chemical names, structural formulas, symbols and molecular weights of the two inhibitor molecules.

Inhibitor	Molecular formula	Structure	Molecular weight ($\text{g}\cdot\text{mol}^{-1}$)
Proline	$\text{C}_5\text{H}_9\text{NO}_2$		115.130
Captopril	$\text{C}_9\text{H}_{15}\text{NO}_3\text{S}$		217.285

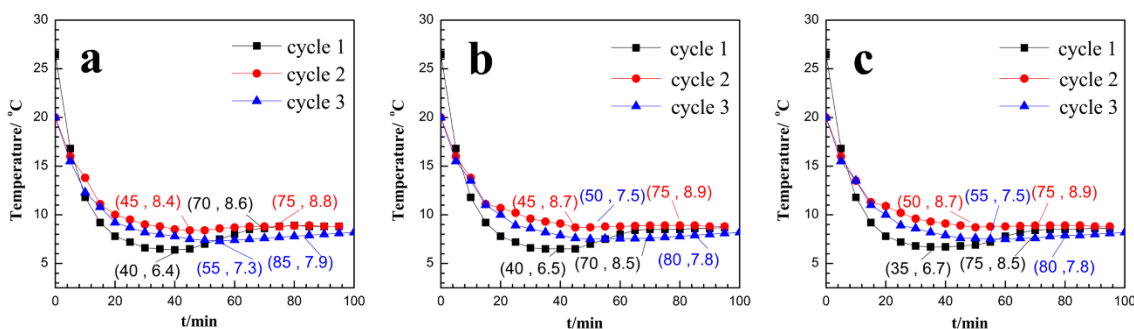


Figure 1. Cooling curves for PCM solutions with and without inhibitors, (a) bare, (b) proline, and (c) captopril.

2.2. Electrodes

Cylindrical carbon steel wrapped with epoxy resin is used as the working electrode, and the exposed area at the bottom end is 0.5024 cm^2 . The chemical composition of the carbon steel is C (0.45 wt.%), Mn (0.5 wt.%), Si (0.17 wt.%), P (0.035 wt.%), S (0.035 wt.%), Cr (0.25 wt.%), Ni (0.30 wt.%), Cu (0.25 wt.%), and Fe for the rest. Before each test, the working electrode should be polished

to a mirror surface with 800#~1400# metallographic sandpaper. The reference electrode is a saturated calomel electrode (SCE). The auxiliary electrode is a piece of platinum with an area of 1 cm².

2.3. Electrochemical measurements

The electrochemical test of the three-electrode test system was carried out at 25 °C using an IM6 electrochemical workstation (ZAHNER, Germany) to study the corrosion inhibition performance of proline and captopril on 1045 carbon steel in a PCM solution. First, the exposed surface of the carbon steel of the working electrode was immersed in the test solution, and the open circuit potential (E_{ocp}) was continuously monitored until, a stable open circuit potential was obtained. Electrochemical impedance spectroscopy was performed at a frequency range of 100 kHz to 0.1 Hz at the stable open circuit potential value, and its signal amplitude perturbation was 5 mV peak-to-peak. Immediately after the EIS test, a potentiodynamic polarization curve was obtained. The potential sweep rate was 2 mV·s⁻¹, and the scan range was $E_{ocp}-200$ mV to $E_{ocp}+200$ mV.

2.4. Surface morphological studies

The polished 1045 carbon steel sheets (5 mm × 5 mm × 1 mm) were completely immersed in PCMs with and without corrosion inhibitor for 120 h. After soaking for a sufficient period of time, the sample was removed and quickly washed with distilled water and dried. Then, the surface topography of the sample was investigated using a field emission scanning electron microscope (HITACHI, SU 5000).

A contact angle test was carried out at three different positions on the surface of the sample by a static contact angle tester (model XG-CAM). The average contact angle value of each sample was calculated, and its hydrophilic/hydrophobic properties were determined.

2.5. Computational

The corrosion inhibition mechanism of the two corrosion inhibitors was calculated and analysed by a quantum chemical calculation and molecular dynamics simulation. In Gaussian 03W software[24], a B3LYP/6-311g(d, p) algorithm and base set conditions are used to optimize the molecular structure and calculate the single point energy of the molecule by the most reasonable density functional theory (DFT) value in the structural optimization module. The highest occupied orbital energy (E_{HOMO}), lowest unoccupied orbital energy (E_{LUMO}), energy gap ($\Delta E = E_{LUMO} - E_{HOMO}$), dipole moment (μ), number of transferred electrons (ΔN) and other quantum chemical parameters, along with a molecular distribution of outer orbits were obtained. The interaction of proline and captopril with the Fe(1 1 0) crystal surface in PCM solution was simulated using the Discover module in Material Studio 6.0 software from Accelrys Inc.[25]. The surface of the Fe(1 1 0) crystal is considered to be the most stable, so that crystal surface is selected as the metal crystal plane for a molecular dynamics simulation. The setting parameters and operation steps of the simulation system of

this experiment refers to the related work of Zhang Zhe[26].

3. RESULTS AND DISCUSSION

3.1. Electrochemical impedance spectroscopy (EIS) measurements

A study was conducted on the corrosion inhibition performance of different concentrations of proline and captopril on 1045 carbon steel in PCM solutions at 25 °C by EIS. The Nyquist diagram and the Bode diagram measured in the two corrosion inhibition systems are shown in Fig. 2. The incomplete semi-circular capacitive reactance arcs of all high frequency regions in Fig. 2(a) and Fig. 2(c) are caused by the heterogeneity and roughness of the working electrode surface[27, 28]. The working electrode has the same shape as the Nyquist curve measured in the PCM solution with and without the corrosion inhibitor, indicating that the carbon steel corrosion process is the same[29, 30]. Fig. 2(b) and Fig. 2(d) show that the phase angle measured in the system with the corrosion inhibitor is greater than the phase angle measured in the system without the corrosion inhibitor. The phase angle measured in a system with the captopril inhibitor is greater than that of the phase angle measured in a system with proline. This indicates that both corrosion inhibitors form a corrosion inhibitor film on the iron surface, and the captopril inhibitor film is more compact and corrosion-resistant than that of the proline corrosion inhibitor film[31, 32].

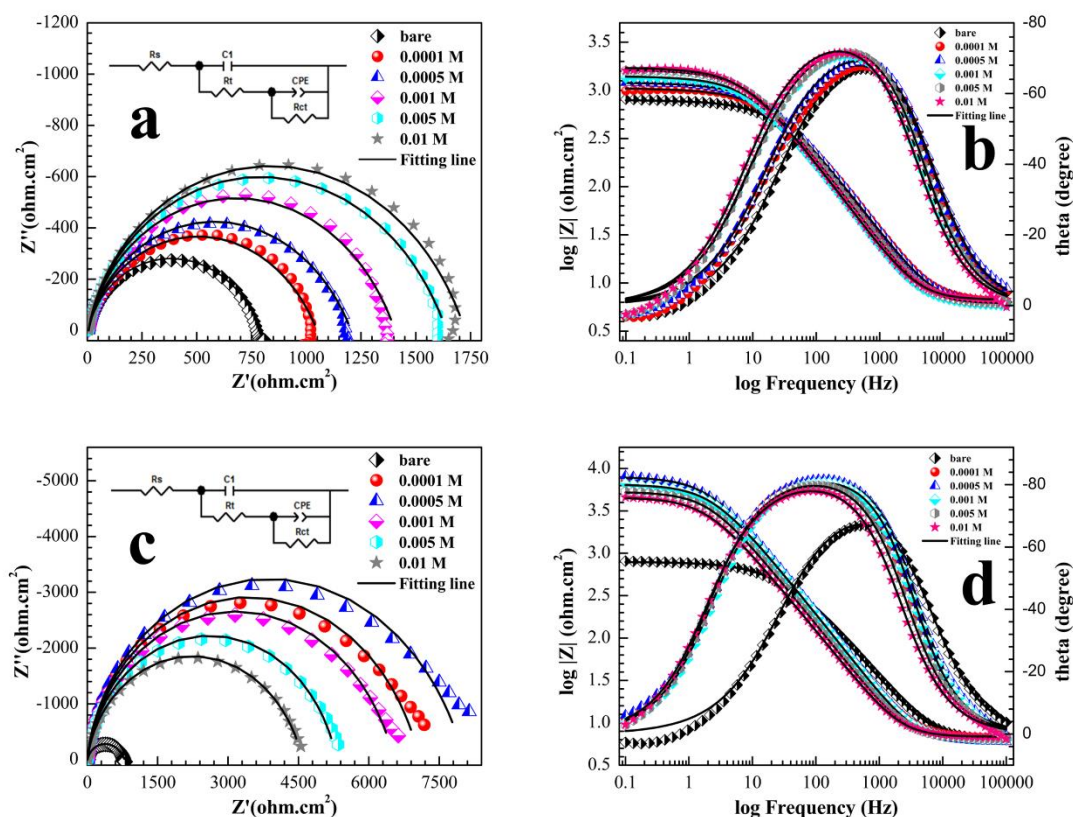


Figure 2. Nyquist plots (a) and (c) and the Bode and phase angle plots (b) and (d) of the carbon steel working electrode in PCM solutions with and without inhibitors at 25 °C.

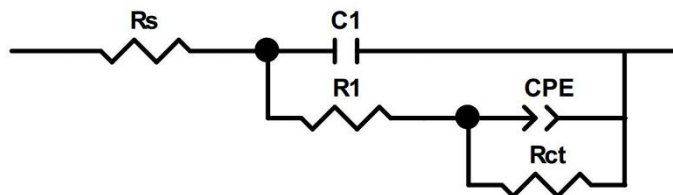


Figure 3. Equivalent circuit diagram used to model the carbon steel working electrode/solution interface in a PCM solution with and without inhibitors at 25 °C.

Table 2. EIS parameters for corrosion of carbon steel in PCM solutions with and without inhibitors at 25 °C.

Inhibitors	Conc. inh (mol L ⁻¹)	R _s (Ω cm ²)	C ₁ (μF cm ⁻²)	R ₁ (Ω cm ²)	CPE		R _{ct} (Ω cm ²)	η _R (%)
					Y ₀ (μΩ ⁻¹ S ⁿ cm ⁻²)	n		
bare	0	6.347±0.71	3.197±2.05	5.488±2.74	30.667±4.64	0.688±1.25	782±0.67	--
	0.0001	6.435±0.77	3.110±2.07	5.409±2.93	30.543±4.46	0.689±1.24	1038±0.77	24.71
	0.0005	6.177±0.59	3.153±1.65	5.258±2.76	28.526±3.29	0.692±0.93	1195±0.58	34.60
	0.001	5.988±0.56	4.801±1.71	5.479±1.78	29.991±3.08	0.718±0.93	1394±0.63	43.94
	0.005	6.198±0.56	4.383±1.65	5.595±2.06	27.167±3.14	0.710±0.97	1630±0.64	52.06
	0.01	6.744±0.58	4.975±1.82	6.227±1.67	26.989±3.27	0.722±1.03	1714±0.69	54.40
Captopril	0.0001	6.809±0.34	6.332±1.10	6.641±1.09	11.113±2.26	0.743±1.07	7078±0.54	88.96
	0.0005	6.157±0.38	6.163±1.03	5.958±1.37	11.102±2.87	0.709±1.35	8047±0.66	90.29
	0.001	6.490±0.30	6.403±0.92	6.261±1.15	12.053±2.15	0.728±0.99	6541±0.49	88.05
	0.005	6.520±0.31	7.756±1.15	6.446±0.81	14.267±1.64	0.781±0.74	5307±0.45	85.27
	0.01	6.882±0.29	8.830±1.03	6.759±0.82	20.583±1.44	0.766±0.62	4579±0.45	82.93

EIS test data were fitted by ZView 2 software. The equivalent circuit (Fig. 3) for fitting consists of a variety of components, such as the solution resistance (R_s) generated between the working electrode and the reference electrode, the electric double layer capacitance (C₁), the charge transfer resistance (R₁) generated between the ion (PO₄³⁻ and SO₄²⁻) concentration layer and the solution, and the charge transfer resistance (R_{ct}) generated between the surface of the working electrode and the solution layer. The parameter values and error values (%) of the components obtained by fitting are shown in Table 2. A CPE is used in the circuit instead of an electric double layer capacitor to account for the deviation caused by the unevenness or roughness of the surface[33-35]. The formula for calculating the admittance (Y) of the CPE is as follows:

$$Y_{CPE} = Y_0(j\omega)^n \tag{1}$$

where Y₀ represents the modulus of the constant phase angle element, and n and ω represent the deviation parameters of the CPE and the frequency corresponding to the maximum phase angle, respectively.

The inhibition efficiency (η_R) of the inhibitor is calculated as follows:

$$\eta \text{ (\%)} = \frac{R_{ct} - R_{ct}^0}{R_{ct}} \times 100 \tag{2}$$

where R_{ct} and R_{ct}^0 represent the charge transfer resistance of the working electrode with and without a corrosion inhibitor, respectively.

Table 2 shows that the values of C_1 and R_1 obtained are small and the change is not obvious. The range of C_1 varies from 3.10 to 8.830 $\mu\text{F}\cdot\text{cm}^{-2}$, and the range of R_1 varies from 5.258 to 6.759 Ω . This indicates that the sulfate and phosphate ion double layer adsorbed or accumulated on the surface of the iron cannot effectively block corrosive ions such as Cl^- ions, and the corrosion inhibition effect is not obvious. In addition, the concentration of proline inhibitor added to the PCM solution was inversely correlated with the Y_0 value and positively correlated with R_{ct} . The decrease in the Y_0 value may be because the corrosion inhibitor molecule replaces the H_2O molecules or other ions adsorbed on the surface of the carbon steel working electrode, resulting in a decrease in the local dielectric constant and/or an increase in the thickness of the electric double layer[26, 36]. When the concentration of captopril inhibitor added to the PCM solution reached $0.0005 \text{ mol}\cdot\text{L}^{-1}$, the measured Y_0 value was the lowest and the R_{ct} value was the highest compared to that of the other samples. This indicates that the optimum concentration of captopril inhibitor is $0.0005 \text{ mol}\cdot\text{L}^{-1}$. When this concentration is exceeded, the corrosion inhibitor molecules may be mutually repelled due to the high molecular content of the corrosion inhibitor. At concentrations lower than $0.0005 \text{ mol}\cdot\text{L}^{-1}$, corrosion inhibitor molecules may not be sufficiently adsorbed on the iron surface due to the low molecular content of the corrosion inhibitor. The value of n (deviation parameters of the CPE) can be used as an indicator to predict the dissolution mechanism[37]. The n values measured in the two systems have no obvious regularity and are relatively stable, and their stability indicates that the dissolution mechanism in the two systems is mainly controlled by the charge transfer process.

3.2. Potentiodynamic polarization measurements

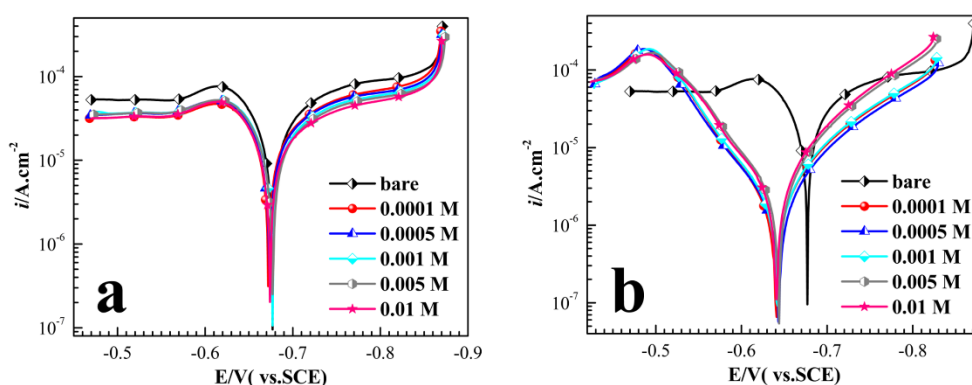


Figure 4. Potentiodynamic polarization curves of carbon steel working electrodes in various concentrations of PCM solution with and without inhibitors at 25 °C: (a) proline inhibitors and (b) captopril inhibitors.

Table 3. Potentiodynamic polarization parameters of proline and captopril inhibitor molecules in PCM solutions with and without inhibitors at 25 °C.

Inhibitors	$Conc.inh$ (mol L ⁻¹)	E_{corr} (V vs.SCE)	$-\beta_c$ (V dec ⁻¹)	β_a (V dec ⁻¹)	i_{corr} ($\mu A cm^{-2}$)	η (%)
bare	0	-0.677	0.428	0.303	48.80	--
Proline	0.0001	-0.671	0.321	0.269	30.00	38.52
	0.0005	-0.673	0.317	0.215	28.80	40.98
	0.001	-0.677	0.306	0.187	26.60	45.49
	0.005	-0.677	0.282	0.145	23.20	52.46
	0.01	-0.675	0.274	0.138	20.60	57.79
Captopril	0.0001	-0.640	0.133	0.090	4.58	90.61
	0.0005	-0.643	0.122	0.087	3.55	92.73
	0.001	-0.641	0.135	0.090	4.92	89.92
	0.005	-0.642	0.135	0.106	8.06	83.48
	0.01	-0.640	0.136	0.117	9.25	81.05

As shown in Fig. 4, the potentiodynamic polarization curve test investigated the corrosion inhibition performance of 1045 carbon steel working electrodes in PCMs with and without corrosion inhibitors. This process was tested and analysed by software provided in the IM6 electrochemical workstation. The original data were fitted by a Tafel extrapolation method. The relevant electrochemical parameters are listed in Table 3, for example, E_{corr} (corrosion potential), i_{corr} (corrosion current density), β_c (cathodic Tafel slopes and β_a (anodic Tafel slopes). The corrosion inhibition efficiency (η_i) is calculated by Eq. (4):

$$\eta_i(\%) = \frac{i_{corr}^0 - i_{corr}}{i_{corr}^0} \times 100 \quad (4)$$

where i_{corr} and i_{corr}^0 represent the corrosion current density of the carbon steel working electrode in the PCM solution with and without corrosion inhibitor, respectively.

As shown in Fig. 4 and Table 3, the working electrode with a corrosion inhibitor has a lower anode and cathode corrosion current density than those of the system without the corrosion inhibitor. This indicates that the inhibitor molecule can adsorb on the surface of the iron to form a corrosion inhibitor film, effectively preventing corrosion from corrosive ions such as Cl⁻ ions. The corrosion potential (E_{corr}) of the working electrode in both corrosion inhibition systems is less than 85 mV (vs. SCE), so both proline and captopril inhibitors are mixed type corrosion inhibitors[20, 38-42]. As shown in Table 3, the addition of the proline inhibitor resulted in a decrease in the corrosion current density (i_{corr}), and the corrosion current density gradually decreased as the concentration increased. This indicates that the amount of proline molecules adsorbed on the surface of the carbon steel working electrode is positively correlated with its concentration. The corrosion inhibitor film can effectively prevent corrosive ions from directly contacting the working electrode, and the degree of corrosion of the carbon steel decreases. When the captopril inhibitor is in the range of 0.0001 mol·L⁻¹~0.0005 mol·L⁻¹, the corrosion current density is inversely proportional to the concentration value, and the corrosion inhibition efficiency is proportional to the concentration value. When the

concentration exceeds $0.0005 \text{ mol}\cdot\text{L}^{-1}$, the corrosion current density is proportional to the concentration value, and the corrosion inhibition efficiency is inversely proportional to the concentration value. This may indicate that when the added amount of captopril inhibitor exceeds a maximum value, a mutual repulsion effect occurs between the inhibitor molecules, resulting in a weakening of the corrosion inhibitor film and a decrease in its corrosion inhibition efficiency. As shown in Table 3, the order of maximum inhibition efficiency for the two corrosion inhibitors was captopril (92.73%) > proline (57.79%). This result is in agreement with the EIS results.

3.3. FESEM characterization and static contact angle analysis

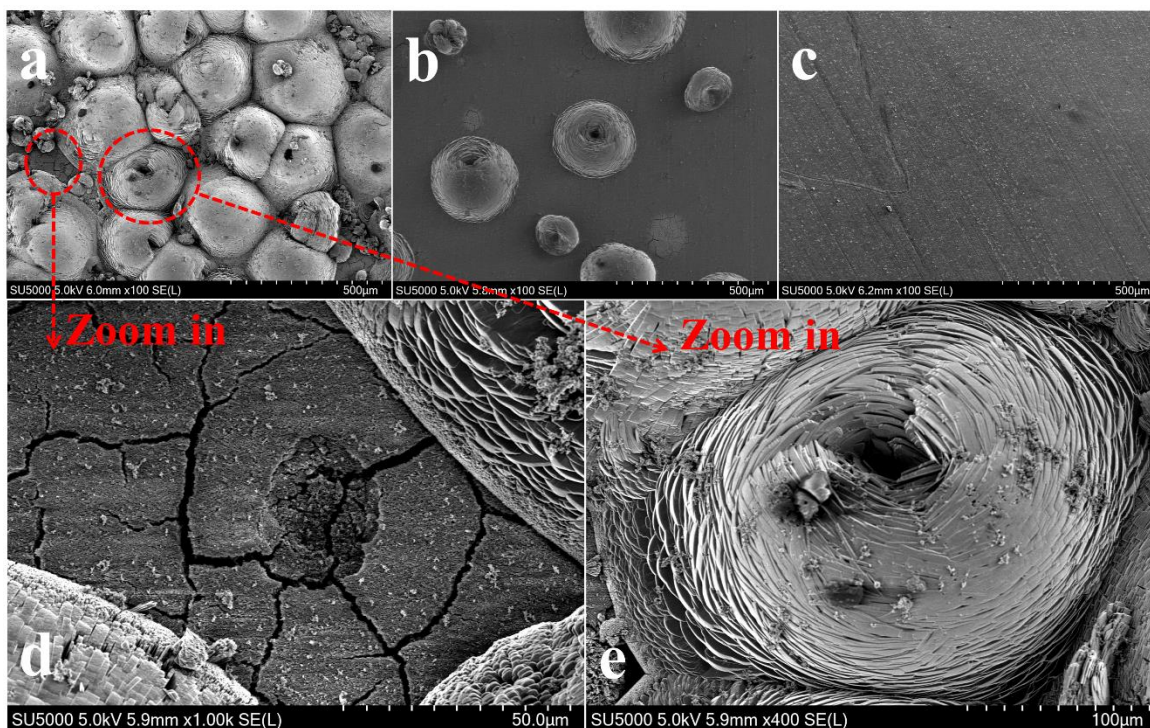


Figure 5. SEM micrographs of corrosion surfaces formed by CS sheets immersed in various PCM solutions for 120 h at 25 °C, (a) blank PCM solution, (b) proline, and (c) captopril. The images in (d) and (e) are magnified views of (a).

Fig. 5 shows the FESEM micromorphology of a carbon steel sheet after soaking for 120 h in a PCM solution with and without a corrosion inhibitor at 25 °C. After the carbon steel sheet is immersed in the blank PCM solution for 120 h, the surface is completely corroded and covered with flake-like corrosion products. At the same time, there are serious corrosion cracks and holes on the surface of carbon steel (as shown in Fig. 5(a), (d) and (e)). The carbon steel that is immersed in the PCM solution with a corrosion inhibitor for 120 h shows that its surface morphology is relatively well preserved. Among them, the iron sheets soaked in the PCM solution with $0.0005 \text{ mol}\cdot\text{L}^{-1}$ captopril inhibitor are more complete than that of the PCMs added with $0.01 \text{ mol}\cdot\text{L}^{-1}$ proline inhibitor, and scratches left by the grinding process can be observed on the surface of the carbon steel sample (as shown in Fig. 5(b) and (c)). After FESEM characterization, it can be concluded that the concentration of $0.0005 \text{ mol}\cdot\text{L}^{-1}$

captopril corrosion inhibitor has a good corrosion inhibition effect.

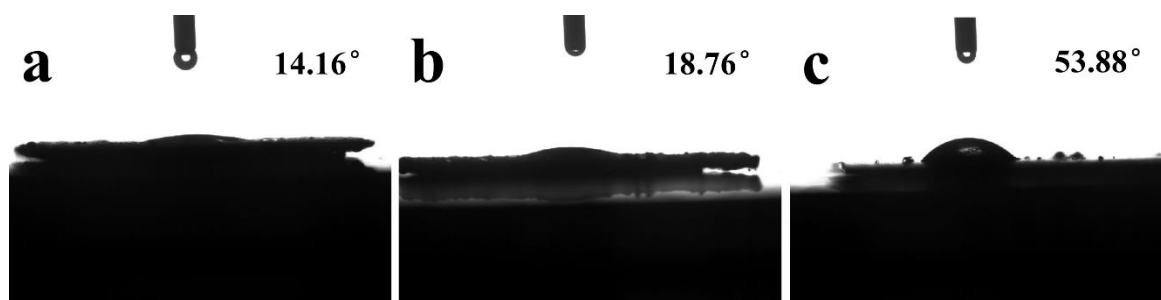


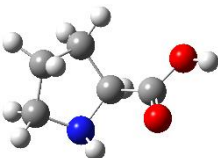
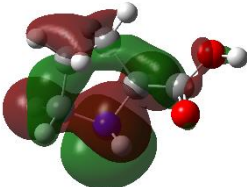
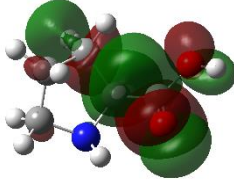
Figure 6. Contact angle test images of corrosion surfaces formed by CS sheets immersed in various PCM solutions for 120 h at 25 °C, (a) blank PCM solution, (b) proline, and (c) captopril.

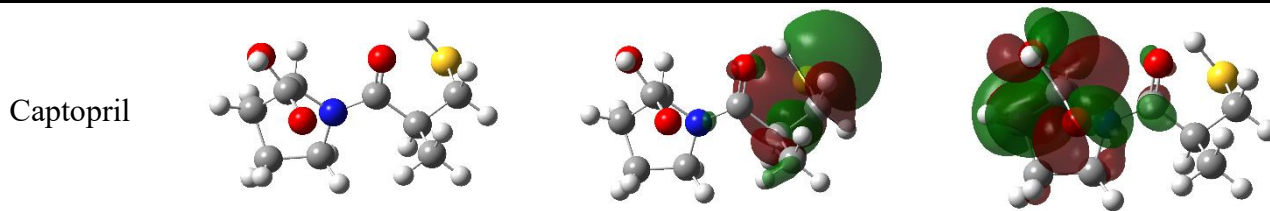
In addition, contact angle tests were performed on carbon steel sheets that had been soaked in PCMs with and without corrosion inhibitors at 25 °C. As shown in Fig. 6, the carbon steel sheet treated with the PCM solution containing the captopril inhibitor had the largest contact angle value (53.88°). This indicates that the captopril inhibitor film formed on the carbon steel sheet is more hydrophobic than that of the proline inhibitor film, and the captopril inhibitor film is more effective in slowing the corrosive ions in the solution.

3.4. Quantum chemical calculation

In this experiment, quantum chemical calculation technology was used to study the correlation between the molecular structure of the corrosion inhibitor molecules and their corrosion inhibition efficiency. Table 4 shows the optimized molecular structure of the two corrosion inhibitor molecules and their HOMO (highest occupied molecular orbital) and LUMO (lowest unoccupied molecular orbital). It can be seen from the molecular orbital diagrams in Table 4 that the HOMOs of proline and captopril molecules are distributed on the N atom and the S atom, respectively. It is shown that the N atom of the proline molecule and the S atom of the captopril molecule can be adsorbed on the iron surface by providing a coordinate bond with the iron atom in the form of a lone pair of electrons. The LUMOs of proline and captopril molecules are mainly distributed on the -COOH group, indicating that the -COOH group is the main site for the two inhibitor molecules to accept foreign electrons.

Table 4. Optimized geometry and frontier molecular orbital density distribution of proline and captopril inhibitor molecules.

Inhibitors	Structure	HOMO	LUMO
Proline			

**Table 5.** Quantum chemical parameters of proline and captopril molecules.

Assembly molecules	E_{HOMO} (eV)	E_{LUMO} (eV)	ΔE (eV)	μ (Debye)	$\chi=(I+A)/2$	$\gamma=(I-A)/2$	ΔN
Proline	-6.240	-0.156	6.084	1.8233	3.198	3.042	0.625
Captopril	-6.458	-0.159	6.299	3.9757	3.309	3.150	0.586

In addition, HOMO energy (E_{HOMO}), LUMO energy (E_{LUMO}), energy gap (ΔE , $\Delta E = E_{LUMO} - E_{HOMO}$), dipole moment (μ) and number of transferred electrons from the inhibitor to the metal surface (ΔN) are important parameters for judging the interaction between the corrosion inhibitor molecule and the metal surface[23, 43, 44]. The values of these parameters are listed in Table 5.

Generally, E_{HOMO} represents the electron donating ability of a compound in a direct proportion. E_{LUMO} represents the ability of a compound to accept electrons in an inverse proportion. ΔE is one of the important parameters reflecting the chemisorption possibility of organic molecules and metal surfaces. If the value of ΔE is lower, the chemical adsorption ability of the corrosion inhibitor molecule on the metal surface is stronger[45-47]. Meanwhile, ΔN represents the electron donating ability of the corrosion inhibitor molecule, and the corrosion inhibition efficiency is proportional to the ΔN value. The ΔN value can be calculated by Eq. (5)[48-50]:

$$\Delta N = \frac{\chi_{Fe} - \chi_{inh}}{2(\gamma_{Fe} + \gamma_{inh})} \quad (5)$$

where χ_{Fe} and γ_{Fe} are the absolute electronegativity and absolute hard sphere index of the iron atom, respectively and according to previous experience, their values are 7 eV and 0 eV, respectively: χ_{inh} and γ_{inh} are the absolute electronegativity and absolute hard sphere index of the corrosion inhibitor molecule, respectively[51, 52].

Ionization potential (I) and electron affinity (A) were calculated by Koopmans theorem and Hartree-Fock theorem, respectively[35, 53, 54]:

$$\chi = \frac{I + A}{2} \quad (6)$$

$$\gamma = \frac{I - A}{2} \quad (7)$$

At the same time, the relationship between E_{HOMO} , E_{LUMO} , I and A was also established. as shown in Eq. (8) and Eq. (9):

$$I = -E_{HOMO} \quad (8)$$

$$A = -E_{LUMO} \quad (9)$$

However, as shown in Table 5, the calculated values of ΔE , ΔN and such are opposite to the experimental results. The results of the quantum chemical calculations do not always correspond to the actual experimental results[55]. Some people believe that the electronic interaction parameters calculated by quantum chemistry should not necessarily be used alone to infer the corrosion inhibition efficiency of corrosion inhibitors[56-59]. They believe that the adsorption of corrosion inhibitors on metal surfaces is a complex process and is not completely determined by a theoretical calculation parameter. It may be necessary to consider some competitive effects. For example, the interaction between molecules, or the interaction between metals and molecules[60].

The dipole moment is a good indicator of the hydrophilic/hydrophobic properties of a molecule[26, 55, 61]. A high dipole moment value indicates the polar character of the molecule and has a hydrophobic character. A low dipole moment represents the non-polar character of the molecule and has hydrophilic properties. As shown in Table 5, the order of dipole moments is captopril (3.9757 Debye) > proline (1.8233 Debye). This indicates that captopril is more hydrophobic than proline, that is, the interaction between captopril and water molecules is stronger than that of proline. Captopril molecules can adsorb and form a good hydrophobic corrosion inhibitor film on the surface of carbon steel, which effectively hinders the further corrosion by other corrosive ions in the aqueous solution. This result is in agreement with the contact angle test results and effectively explains the electrochemical test results.

3.5. Molecular Dynamic simulation

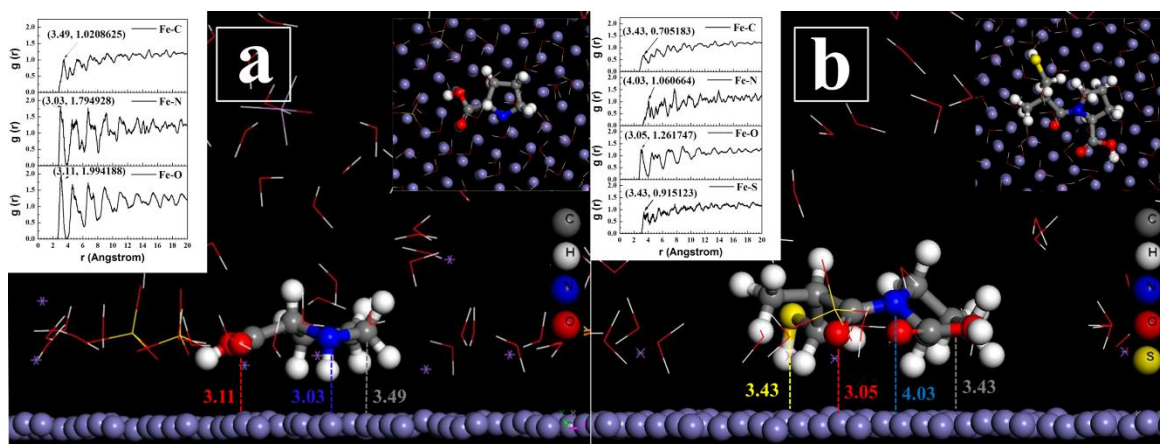


Figure 7. Molecular simulation of the most favourable adsorption mode obtained by the inhibitors on the Fe (1 1 0) surface in PCM solution: (a) proline and (b) captopril.

As shown in Fig 7, molecular dynamics simulations were used to study the adsorption behaviour of proline and captopril on the Fe (1 1 0) surface, which can predict the most favourable configuration for adsorption of the two inhibitor molecules on the iron surface. At the same time, the radial distribution function between the different elements in the corrosion inhibitor molecule and the Fe (1 1 0) crystal plane is also obtained. The shortest bond length values between the C atoms, N atoms, O atoms, S atoms and the Fe (1 1 0) face of the two corrosion inhibitor molecules are as

follows:

Proline-Fe adsorption model: (C-Fe = 3.49 Å, N-Fe = 3.03 Å, O-Fe = 3.11 Å);

Captopril-Fe adsorption model: (C-Fe = 3.43 Å, N-Fe = 4.03 Å, O-Fe = 3.05 Å, S-Fe = 3.43 Å);

Generally, if the bond length is less than 3.5 Å, a strong chemical bond is formed between the atoms[62]. In contrast, it shows that van der Waals forces are the main interaction forces. The C-Fe, N-Fe, and O-Fe bond in the proline inhibitor molecule and the C-Fe, O-Fe and S-Fe bonds in the captopril inhibitor are all less than 3.5 Å. It is indicated that the N, O atoms in the proline molecule and the O and S atoms in the captopril molecule can provide a certain number of lone pairs of electrons to the empty d orbital of iron and form stable coordinate bonds with the iron surface. The bond length of the N-Fe bond in the captopril molecule is 4.03 Å, which is greater than 3.5 Å. This indicates that the captopril molecule in the PCM solution cannot be adsorbed on the iron surface with the N atom as the active site, which may be caused by the enrichment of sulfate ions and phosphate ions on the iron surface.

When the molecular dynamics simulation system is balanced in temperature and energy, the binding energy ($E_{binding}$) and adsorption energy ($E_{adsorption}$) between the corrosion inhibitor molecule and the Fe (1 1 0) surface are calculated. These parameters can be used to evaluate the adsorption strength of the corrosion inhibitor molecules on the surface of the carbon steel. The equilibrium adsorption parameters obtained by the molecular dynamic simulation are shown in Table 6. The formula for the adsorption energy ($E_{adsorption}$) and binding energy ($E_{binding}$) of the solution simulation system is as follows:

$$E_{adsorption} = E_{total} - (E_{surface+solution} + E_{inhibitor+solution}) + E_{solution} \quad (10)$$

$$E_{binding} = -E_{adsorption} \quad (11)$$

where E_{total} is the total potential energy of the whole simulation system, $E_{surface+solution}$ is the total potential energy of the simulation system without corrosion inhibitor molecules, and $E_{inhibitor+solution}$ is the total potential energy of the simulation system without iron surface, $E_{solution}$ represents the energy of the PCM solution.

Table 6. Adsorption and binding energies of the proline and captopril inhibitor molecules to the Fe (1 1 0) surface in the simulated system.

Inhibitors	$E_{adsorption}$ (eV)	$E_{binding}$ (eV)	η_{max} (%)
Proline	-2.706	2.706	57.79
Captopril	-4.443	4.443	92.73

As shown in Table 6, the order of the binding energy of the inhibitor captopril (4.443 eV) > proline (2.706 eV). An increased $E_{binding}$ value means a more stable adsorption system and an increased corrosion inhibition efficiency of the corrosion inhibitor as calculated by theoretical analysis, namely: $\eta_{max(captopril)} > \eta_{max(proline)}$. This is consistent with the electrochemical test results.

Cl⁻ ions have a small ionic radius, strong penetrating ability, and strong adsorption capacity with metal materials; the strong adsorption can lead to forming soluble chloride with metals, which can cause and accelerate the corrosion reaction of carbon steel in corrosive media[26, 61]. In view of the large amount of Cl⁻ ions in the PCM solution, we used molecular dynamics simulation techniques to study and calculate the diffusion coefficients of Cl⁻ ions in a simulation system with two inhibitors. In addition, to verify the hydrophilic/hydrophobic properties of the two corrosion inhibitors, we also simulated and calculated the diffusion coefficients of H₂O molecules in the system.

Generally, a low diffusion coefficient (D) value of the corrosive ions means a good corrosion inhibiting effect of the corrosion inhibitor. The calculation for the diffusion coefficient (D) of corrosive ions in the system is shown in Eq. (12) and Eq. (13)[63-67]:

$$MSD(t) = \left[\frac{1}{N} \sum_{i=1}^N |R_i(t) - R_i(0)|^2 \right] \tag{12}$$

$$D = \frac{1}{6} \lim_{t \rightarrow \infty} \frac{d}{dx} \sum_i^n \left[|R_i(t) - R_i(0)|^2 \right] \tag{13}$$

where *N* is the number of target molecules, *R_i(t)* and *R_i(0)* are the positions of the corrosive ions at time *t* and 0, respectively, and $|R_i(t) - R_i(0)|^2$ represents the mean square displacement (MSD).

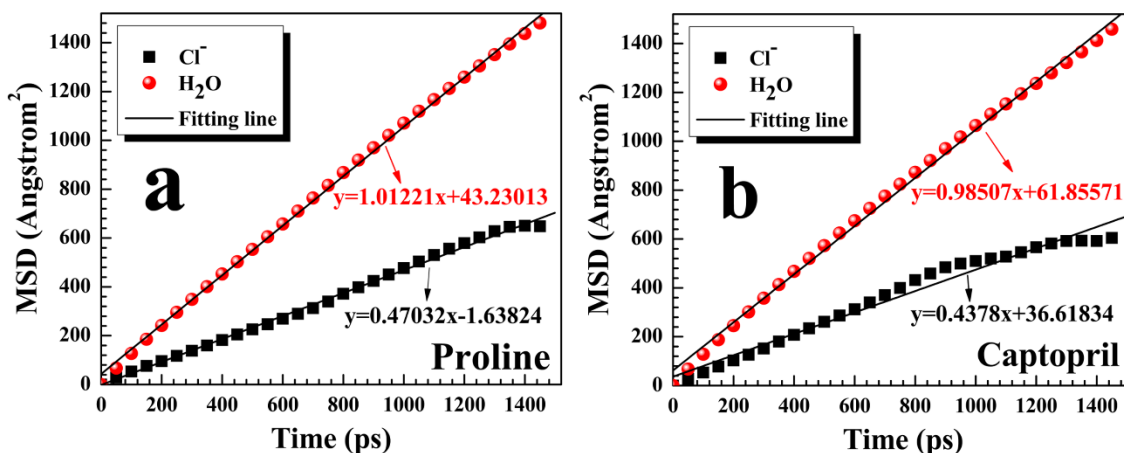


Figure 8. The MSD curves of Cl⁻ ions and H₂O molecules corrosive species in the two kinds of dynamic simulation systems.

Table 7. The diffusion coefficient of Cl⁻ ions and H₂O molecules in the two kinds of dynamic inhibitor film simulation systems.

Inhibitors	Diffusion coefficient / (10 ⁻⁹ m ² s ⁻¹)		η _{max} (%)
	Cl ⁻	H ₂ O	
Proline	0.078387	0.168702	57.79
Captopril	0.072967	0.164178	92.73

It can be clearly seen from Fig. 8 and Table 7 that the magnitude of the migration rate values of Cl⁻ ions and H₂O molecules in both systems are: captopril < proline, indicating that the corrosion inhibition effect of captopril is better than that of proline. At the same time, it was also verified that the

captropril molecule is more hydrophobic than proline. Captropril molecules can form a layer of hydrophobic corrosion inhibitor film on the surface of carbon steel, which effectively hinders further corrosion from other corrosive ions in aqueous solution.

This is consistent with the results of the contact angle test and quantum chemical calculations.

In addition, the concentration profiles of Cl^- ions and H_2O molecules in the normal direction of the iron surface (0 0 1) were also analysed with a surface concentration profile curve. The results are shown in Fig. 9. The profiles of Cl^- ions and H_2O molecules in the captropril inhibitor simulation system are farther than those in the proline inhibitor simulation system, indicating that captropril inhibitors are a good barrier to Cl^- ions and H_2O molecules, thus, making it more difficult for those molecules to access the carbon steel surfaces.

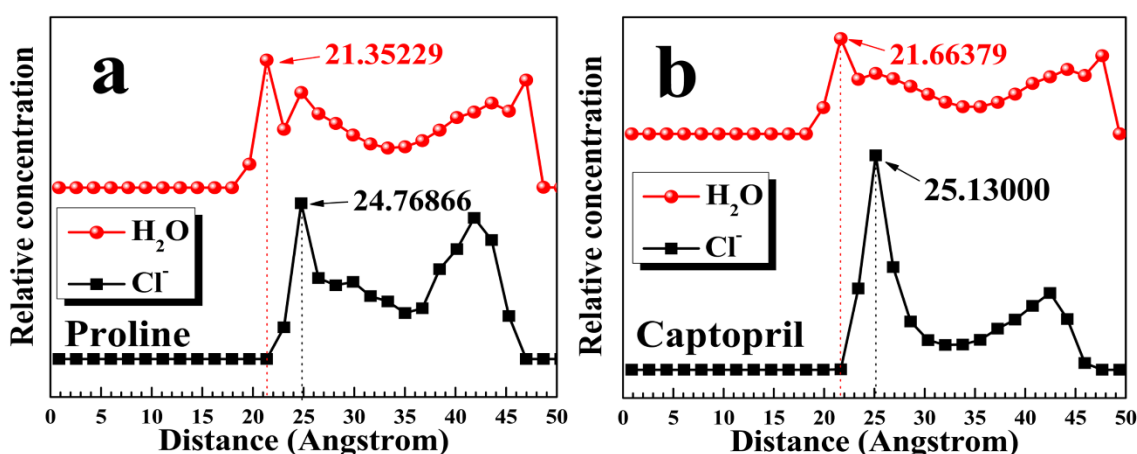


Figure 9. The surface concentration profile curves of Cl^- ions and H_2O molecules as corrosive species in the two kinds of dynamic simulation systems in the normal (0 0 1) direction.

4. CONCLUSION

The inhibition performance of proline and captropril on 1045 carbon steel in PCM solution has been studied. From the electrochemical test results, both proline and captropril inhibitors have a corrosion inhibition effect. The corrosion inhibition efficiency of the proline inhibitor increased with the concentration value, and the highest inhibition efficiency was 57.79%. When the concentration of captropril inhibitor is $0.0001\sim 0.0005\text{ mol}\cdot\text{L}^{-1}$, the inhibition efficiency is directly proportional to the concentration. When the concentration of captropril inhibitor is $0.0005\sim 0.01\text{ mol}\cdot\text{L}^{-1}$, the inhibition efficiency is negatively correlated with the concentration. Finally, when the concentration of captropril inhibitor is $0.0005\text{ mol}\cdot\text{L}^{-1}$, the inhibition efficiency is the highest, i.e., 92.73%. Captropril has the advantages of a low dose and high corrosion inhibition efficiency and can be used as an economical and efficient corrosion inhibitor for PCMs. The potentiodynamic polarization test showed that both proline and captropril were mixed corrosion inhibitors, and the inhibition efficiency effect was the same as that of the EIS test.

FESEM characterization tests confirmed that the two corrosion inhibitors have a certain inhibitory effect on carbon steel in PCM solutions. The surface morphology of the carbon steel sample soaked with captopril inhibitor and the surface morphology of the carbon steel immersed in the blank PCM solution are quite different, and the corrosion is greatly reduced on the former. Thus, captopril has a good corrosion inhibition effect. The contact angle test results show that the captopril corrosion inhibitor is more hydrophobic than proline, which can slow the corrosion of 1045 carbon steel in PCMs.

Theoretical calculations show that both proline and captopril inhibitors can form a corrosion inhibitor film on the surface of Fe (1 1 0). The N atoms, S atoms and -COOH groups in the corrosion inhibitor are the main adsorption active sites. The adsorption capacity of the captopril molecule on the Fe (1 1 0) surface is stronger than that of the proline. In addition, the diffusion coefficients and surface concentration profiles of Cl⁻ ions and H₂O molecules in the two systems were also calculated by simulation. The corrosion inhibition mechanism of the two corrosion inhibitors was analysed with the data verifying that the corrosion inhibition effect of the captopril inhibitor on 1045 carbon steel in PCM solution was better than that of proline.

ACKNOWLEDGEMENTS

This work was funded by the Nature Science Foundation of Guangxi Province of China (No. 2016GXNSFAA380061) and the Guangxi Key Laboratory of Electrochemical and Magnetochemical Functional Materials (EMFM20161104, EMFM20161203).

References

1. M.E. Zayed, J. Zhao, A.H. Elsheikh, Y. Du, F.A. Hammad, L. Ma, A.E. Kabeel, S. Sadek, *Process Saf. Environ. Prot.*, 128 (2019) 135-157.
2. Q. Li, W. Moya, I. Janghorban Esfahani, J. Rashidi, C. Yoo, *Process Saf. Environ. Prot.*, 111 (2017) 795-809.
3. A.E. Kabeel, A. Khalil, S.M. Shalaby, M.E. Zayed, *Energy Convers. Manage.*, 113 (2016) 264-272.
4. Z. Khan, Z. Khan, A. Ghafoor, *Energy Convers. Manage.*, 115 (2016) 132-158.
5. L. Ma, Y. Li, J. Wang, S. Li, J. Zhao, W. Li, M.E. Zayed, Q. Shao, M. Sun, *Energy and Buildings*, 194 (2019) 218-231.
6. A. Shehzad, M.J.K. Bashir, S. Sethupathi, J.-W. Lim, *Process Saf. Environ. Prot.*, 98 (2015) 309-318.
7. S.W. Sharshir, A.H. Elsheikh, G. Peng, N. Yang, M.O.A. El-Samadony, A.E. Kabeel, *Renewable Sustainable Energy Rev.*, 73 (2017) 521-544.
8. G.R. Dheep, A. Sreekumar, *Appl. Therm. Eng.*, 129 (2018) 1189-1196.
9. M.T. de Miguel, V. Encinas-Sánchez, M.I. Lasanta, G. García-Martín, F.J. Pérez, *Sol. Energy Mater. Sol. Cells*, 157 (2016) 966-972.
10. Y. Grosu, O. Bondarchuk, A. Faik, *Sol. Energy Mater. Sol. Cells*, 174 (2018) 34-41.
11. S. Guillot, A. Faik, A. Rakhmatullin, J. Lambert, E. Veron, P. Echegut, C. Bessada, N. Calvet, X. Py, *Appl. Energy*, 94 (2012) 174-181.
12. A.G. Fernández, H. Galleguillos, E. Fuentealba, F.J. Pérez, *Sol. Energy Mater. Sol. Cells*, 141 (2015) 7-13.
13. G. Ferrer, A. Solé, C. Barreneche, I. Martorell, L.F. Cabeza, *Renewable Energy*, 76 (2015) 465-469.
14. K. Vignarooban, P. Pugazhendhi, C. Tucker, D. Gervasio, A.M. Kannan, *Sol. Energy*, 103 (2014)

- 62-69.
15. E. Oró, L. Miró, C. Barreneche, I. Martorell, M.M. Farid, L.F. Cabeza, *Appl. Energy*, 109 (2013) 449-453.
 16. M.C. Browne, E. Boyd, S.J. McCormack, *Renewable Energy*, 108 (2017) 555-568.
 17. P. Moreno, L. Miró, A. Solé, C. Barreneche, C. Solé, I. Martorell, L.F. Cabeza, *Appl. Energy*, 125 (2014) 238-245.
 18. L. Hamadi, S. Mansouri, K. Oulmi, A. Kareche, *Egypt. J. Pet.*, 27 (2018) 1157-1165.
 19. B. El Ibrahimy, A. Jmiai, L. Bazzi, S. El Issami, *Arabian J. Chem.*, (2017).
 20. K. Zhang, W. Yang, X. Yin, Y. Chen, Y. Liu, J. Le, B. Xu, *Carbohydr. Polym.*, 181 (2018) 191-199.
 21. L.K.M.O. Goni, M.A.J. Mazumder, S.A. Ali, M.K. Nazal, H.A. Al-Muallem, *Int. J. Miner., Metall. Mater.*, 26 (2019) 467-482.
 22. M.A. Jafar Mazumder, L.K.M.O. Goni, S.A. Ali, M.K. Nazal, *Iran. Polym. J.*, 27 (2018) 979-995.
 23. V. Srivastava, J. Haque, C. Verma, P. Singh, H. Lgaz, R. Salghi, M.A. Quraishi, *J. Mol. Liq.*, 244 (2017) 340-352.
 24. M. J. Frisch, G. W. Trucks, H. B. Schlegel, G. E. Scuseria, M. A. Robb, J. R. Cheeseman, J. A. Montgomery, Jr., T. Vreven, K. N. Kudin, J. C. Burant, J. M. Millam, S. S. Iyengar, J. Tomasi, V. Barone, B. Mennucci, M. Cossi, G. Scalmani, N. Rega, G. A. Petersson, H. Nakatsuji, M. Hada, M. Ehara, K. Toyota, R. Fukuda, J. Hasegawa, M. Ishida, T. Nakajima, Y. Honda, O. Kitao, H. Nakai, M. Klene, X. Li, J. E. Knox, H. P. Hratchian, J. B. Cross, C. Adamo, J. Jaramillo, R. Gomperts, R. E. Stratmann, O. Yazyev, A. J. Austin, R. Cammi, C. Pomelli, J. W. Ochterski, P. Y. Ayala, K. Morokuma, G. A. Voth, P. Salvador, J. J. Dannenberg, V. G. Zakrzewski, S. Dapprich, A. D. Daniels, M. C. Strain, O. Farkas, D. K. Malick, A. D. Rabuck, K. Raghavachari, J. B. Foresman, J. V. Ortiz, Q. Cui, A. G. Baboul, S. Clifford, J. Cioslowski, B. B. Stefanov, G. Liu, A. Liashenko, P. Piskorz, I. Komaromi, R. L. Martin, D. J. Fox, T. Keith, M. A. Al-Laham, C. Y. Peng, A. Nanayakkara, M. Challacombe, P. M. W. Gill, B. Johnson, W. Chen, M. W. Wong, C. Gonzalez, and J. A. Pople, Gaussian, Inc., Wallingford CT, 2004.
 25. Materials Studio, Revision 6.0, Accelrys Inc., San Diego, USA, 2011.
 26. Z. Zhang, W. Li, W. Zhang, X. Huang, L. Ruan, L. Wu, *J. Mol. Liq.*, 272 (2018) 528-538.
 27. X. Luo, C. Ci, J. Li, K. Lin, S. Du, H. Zhang, X. Li, Y.F. Cheng, J. Zang, Y. Liu, *Corros. Sci.*, 151 (2019) 132-142.
 28. R. Sadeghi Erami, M. Amirnasr, S. Meghdadi, M. Talebian, H. Farrokhpour, K. Raeissi, *Corros. Sci.*, 151 (2019) 190-197.
 29. Z. Zhang, N. Tian, X. Li, L. Zhang, L. Wu, Y. Huang, *Appl. Surf. Sci.*, 357 (2015) 845-855.
 30. Z. Zhang, N.C. Tian, X.D. Huang, W. Shang, L. Wu, *RSC Adv.*, 6 (2016) 22250-22268.
 31. R. Yıldız, *Corros. Sci.*, 90 (2015) 544-553.
 32. C.-c. Li, X.-y. Guo, S. Shen, P. Song, T. Xu, Y. Wen, H.-F. Yang, *Corros. Sci.*, 83 (2014) 147-154.
 33. M. Izadi, T. Shahrabi, B. Ramezanzadeh, *Appl. Surf. Sci.*, 440 (2018) 491-505.
 34. R. Fuchs-Godec, M.G. Pavlović, *Corros. Sci.*, 58 (2012) 192-201.
 35. Z. Salarvand, M. Amirnasr, M. Talebian, K. Raeissi, S. Meghdadi, *Corros. Sci.*, 114 (2017) 133-145.
 36. J. Aljourani, K. Raeissi, M.A. Golozar, *Corros. Sci.*, 51 (2009) 1836-1843.
 37. M. Ozcan, *Acta Phys.-Chim. Sin.*, 24 (2008) 1387-1392.
 38. E. Kowsari, S.Y. Arman, M.H. Shahini, H. Zandi, A. Ehsani, R. Naderi, A. PourghasemiHanza, M. Mehdipour, *Corros. Sci.*, 112 (2016) 73-85.
 39. M.K. Pavithra, T.V. Venkatesha, M.K. Punith Kumar, H.C. Tondan, *Corros. Sci.*, 60 (2012) 104-111.
 40. M.A. Bedair, A.S. Fouda, M.A. Ismail, A. Mostafa, *Ionics*, 25 (2018) 2913-2933.
 41. L.L. Liao, S. Mo, H.Q. Luo, N.B. Li, *J. Colloid Interface Sci.*, 499 (2017) 110-119.
 42. Y. Qiang, S. Zhang, S. Xu, W. Li, *J. Colloid Interface Sci.*, 472 (2016) 52-59.
 43. I.B. Obot, D.D. Macdonald, Z.M. Gasem, *Corros. Sci.*, 99 (2015) 1-30.

44. C. Zhu, H.X. Yang, Y.Z. Wang, D.Q. Zhang, Y. Chen, L.X. Gao, *Ionics*, 25 (2018) 1395-1406.
45. L.M. Rodríguez-Valdez, W. Villamizar, M. Casales, J.G. González-Rodríguez, A. Martínez-Villafañe, L. Martinez, D. Glossman-Mitnik, *Corros. Sci.*, 48 (2006) 4053-4064.
46. I. Ahamad, R. Prasad, M.A. Quraishi, *Mater. Chem. Phys.*, 124 (2010) 1155-1165.
47. S.A. Umoren, I.B. Obot, Z.M. Gasem, *Ionics*, 21 (2014) 1171-1186.
48. F. Zhang, Y. Tang, Z. Cao, W. Jing, Z. Wu, Y. Chen, *Corros. Sci.*, 61 (2012) 1-9.
49. I.B. Obot, Z.M. Gasem, *Corros. Sci.*, 83 (2014) 359-366.
50. R. Yıldız, *Ionics*, 25 (2018) 859-870.
51. I.B. Obot, N.O. Obi-Egbedi, E.E. Ebenso, A.S. Afolabi, E. E Oguzie, *Res. Chem. Intermed.*, 39 (2012) 1927-1948.
52. S. Deng, X. Li, X. Xie, *Corros. Sci.*, 80 (2014) 276-289.
53. S. Kaya, L. Guo, C. Kaya, B. Tüzün, I.B. Obot, R. Tourir, N. Islam, *J. Taiwan Inst. Chem. Eng.*, 65 (2016) 522-529.
54. T. Koopmans, *Physica*, 1 (1933) 104-113.
55. E.E. Ebenso, M.M. Kabanda, L.C. Murulana, A.K. Singh, S.K. Shukla, *Ind. Eng. Chem. Res.*, 51 (2012) 12940-12958.
56. E.-S.M. Sherif, *J. Ind. Eng. Chem.*, 19 (2013) 1884-1889.
57. R. Solmaz, G. Kardaş, M. Çulha, B. Yazıcı, M. Erbil, *Electrochim. Acta*, 53 (2008) 5941-5952.
58. Sudheer, M.A. Quraishi, *Corros. Sci.*, 70 (2013) 161-169.
59. J. Światowska, P. Volovitch, K. Ogle, *Corros. Sci.*, 52 (2010) 2372-2378.
60. Z. Tao, S. Zhang, W. Li, B. Hou, *Corros. Sci.*, 51 (2009) 2588-2595.
61. Z. Zhang, N. Tian, W. Zhang, X. Huang, L. Ruan, L. Wu, *Corros. Sci.*, 111 (2016) 675-689.
62. S.K. Saha, P. Banerjee, *RSC Adv.*, 5 (2015) 71120-71130.
63. Y. Yan, X. Wang, Y. Zhang, P. Wang, X. Cao, J. Zhang, *Corros. Sci.*, 73 (2013) 123-129.
64. A. Guo, G. Duan, K. He, B. Sun, C. Fan, S. Hu, *Comput. Theor. Chem.*, 1015 (2013) 21-26.
65. X.Y. Zhang, Q.X. Kang, Y. Wang, *Comput. Theor. Chem.*, 1131 (2018) 25-32.
66. S. Hu, A. Guo, Y. Geng, X. Jia, S. Sun, J. Zhang, *Mater. Chem. Phys.*, 134 (2012) 54-60.
67. L. Guo, S. Kaya, I.B. Obot, X. Zheng, Y. Qiang, *J. Colloid Interface Sci.*, 506 (2017) 478-485.